Ultrasensitive Single Extracellular Vesicle Detection Using High Throughput Droplet Digital Enzyme-Linked Immunosorbent Assay

Zijian Yang[1, ‡], Yasemin Atiyas[2, ‡], Hanfei Shen[2, ‡], Michael J. Siedlik[2], Jingyu Wu [3], Kryshawna Beard[4], Gennadiy Fonar[5], Jean Pierre Dolle[5], Douglas H. Smith[5], James H. Eberwine[4], David F. Meaney[2], David A. Issadore[2,6]

[1] Department of Mechanical Engineering and Applied Mechanics, School of Engineering and Applied Science, University of Pennsylvania, Philadelphia, Pennsylvania, United States

[2] Department of Bioengineering, School of Engineering and Applied Science, University of Pennsylvania, Philadelphia, Pennsylvania, United States

[3] Department of Chemical and Biomolecular Engineering, University of Pennsylvania, Philadelphia, Pennsylvania, United States

[4] Department of Pharmacology, Perelman School of Medicine, University of Pennsylvania, Philadelphia, Pennsylvania, United States

[5] Center for Brain Injury & Repair, Department of Neurosurgery, University of Pennsylvania, Philadelphia, Pennsylvania, United States

[6] Department of Electrical and Systems Engineering, School of Engineering and Applied Science, University of Pennsylvania, Philadelphia, Pennsylvania, United States

‡ These authors contribute equally to the work

Corresponding Author

David A. Issadore

Department of Bioengineering, Department of Electrical and Systems Engineering, and Department of Chemical and Biomolecular Engineering

University of Pennsylvania, Philadelphia, Pennsylvania 19104, United States;

Email: issadore@seas.upenn.edu

Supplementary Information

METHODS

Microfluidic Device Fabrication

DEVA consists several components to enable high throughput droplet base single EV detection (Figure 1C): (a) parallelized droplet generators that partition the mixture of bead and HRP substrate into picolitre sized droplets, (b) a delay line for enzymatic amplification reaction, and (c) the parallelized microfluidic channel where fluorescence signal is recorded. All microfluidic devices used in this work were fabricated using standard soft lithography. A thin layer of SU8 (MicroChem) was first spin coated on top of a silicon wafer. The spin rate was altered based on the targeted height. The SU8 later was then patterned via standard photolithography process: UV exposure, development, and baking. Afterwards, the wafer with patterned SU8 was silanized to complete the mold fabrication process. PDMS was well mixed with curing agent at a 10:1 ratio, poured onto the wafer with the SU8 mold, and degassed until there was no visible air bubbles. Then the PDMS was placed into a 65℃ over for at least 1 hour. The PDMS piece was eventually cut off from the mold. Holes for inlet and outlets were punched by a 1.5mm disposable biopsy punch (INTERGRA). The assembly of the PDMS microfluidic device was conducted in the University of Pennsylvania's Nanofabrication facility, The Singh Center. First, conventional soft lithography was used to fabricate Si/SU-8 molds and PDMS replicates with microfluidic droplet generators. Also using conventional soft lithography, we fabricated Si/Su-8 molds and PDMS replicates that contain with microfluidic droplet generators and channels for droplet incubation and fluorescence detection. The design files are included separately. The two PDMS pieces and a glass substrate were subsequently treated with an oxygen plasma (Anatech SCE-106 Barrel Asher) at 100 W for 30 seconds, aligned, and bonded. Alignment was done manually under a stereoscope. To make the µfluidic channel hydrophobic, we treated the devices with 1% silane (Trichloro(1H,1H,2H,2H-

perfluorooctyl)silane; Sigma) diluted in HFE 7500 Engineering Fluid (3M) for 1 hour and then flush the

channel by HFE 7500 Engineering Fluid.

Optical setup

DEVA's detection device is placed in a laser-cut acrylic chip(1/8") holder that aligns the chip under the RGB machine vision camera (Grasshopper3 USB3, GS3-U3-23S6C-C; FLIR). The chip is illuminated by blue and green lasers housed in an RGB laser module (λ_{exBlue} = 457 nm, 3.66 W; $\lambda_{exGreen}$ = 528 nm, 1.25 W; Techhood), in which laser beams are guided by dichroic mirrors to exit through a single aperture. The collinear laser beams pass through a 20° circle tophat diffuser (ED1-C20-MD; Thorlabs) as they exit the module, creating a ~20 mm diameter spotlight that illuminates the entire 15x9 mm^2 field of view uniformly. The emitted light from the detection device passes through a multi-bandpass filter (λ_{cwl} = 485 ± 10 nm, 559.5 ± 12.5 nm, FF01-387/485/559/649-25; Semrock) and a C-mount macro zoom lens (MLM3X-MP; Computar) as it reaches the camera. The light sources are driven using a TTL module and a microcontroller (Arduino Mega2560) that modulates each laser according to its unique MLS pattern and triggers the camera to begin exposure in phase with the MLS. The MLS patterns were selected as described previously(*1*, *2*). The videos of flowing droplets are taken using the FlyCap2 software (2.11.3.121; Point Grey Research) and stored locally for subsequent processing and analysis.

Human Neuron Cell Culture

Human iPS cells were differentiated into neurons using an established protocol(*3*). Briefly, iPS cells were infected with two lentiviral vectors: TetO-mNgn2-T2A-PuroR and Ubiq-rTTA. Neuronal differentiation was initiated by exposure to 2ug/ml doxycycline (Sigma), followed 24hrs later by 5ug/ml puromycin (Sigma) selection for cells that possessed these two lentiviral vectors. Differentiating cells were then plated on a deformable silicone membrane (0.002-in. thickness, Specialty Manufacturing) at a density of 60,000 cells/ml, that was precoated with Matrigel (Sigma) (*4*). Cells were grown in Neurobasal-A medium (Gibco) with B27 (Life Technologies), glutamax (Life technologies), 5 mM glucose, 10 mM sodium pyruvate, 10 ng/ml NT-3 (Peprotech), 10 ng/ml Brain-derived neurotrophic factor (Peprotech), and 2 µg/ml doxycycline. Differentiated neurons were cultured for 18 days. Doxycycline was discontinued on day 10. Media was changed every 3 or 4 days where it was collected and stored at -20°C.

Preparation of Antibody Coated Magnetic Microbeads and Detection Antibody Biotinylation

Capture antibody (anti-human CD81 antibody, 130-124-538, Miltenyi) was coated on the surface of 5.4 µm Fluorescent Yellow Carboxyl Magnetic Particles (FCM-5052-2, Spherotech) following the protocol from PolyLink Protein Coupling Kit (24350-1, Polyscience). Briefly, we activated the carboxyl groups on the microbeads by water soluble carbodiimide (EDAC). The carbodiimide reacts with the carboxyl group and creates an active ester that is reactive towards primary amines on the capture antibody.

Detection antibodies were biotinylated following the protocol of one-step antibody biotinylation kit (Miltenyi). Briefly, anti-human CD81 antibody (130-124-538, Miltenyi) was prepared at the concentration of 100 µg/mL in PBS. 100 µL of CD81 detection antibody was added into one Miltenyi well containing lyophilized powder. The solution was suspended repeatedly to mix the lyophilized powder thoroughly. The mixture was incubated at room temperature for 24 hours before usage.

Video Processing and Analysis

This droplet detection workflow relies on modulating the excitation sources with a pseudorandom sequence at a rate greater than the frame rate of the camera, which enables the moving fluorescent beads and droplets to be imaged as patterned streaks. Correlating the fluorescence signal of the patterned droplet with the expected sequence results in a distinct peak and enables an individual droplet to be resolved amongst neighboring droplets, with a minimum separation of 3.5 times the droplet diameter(*2*). Simulation experiments and subsequent receiver operator characteristic (ROC) analysis, in which the number of droplets per channel is gradually increased from N=1 to N=27, reveal that as many as 20 patterned droplets can be detected in a single channel with an area under the curve (AUC) > 0.95 (*2*). The length of the droplet streak L_{streak} is set to be 1/3 of the channel length according to the equation $L_{streak} = v \: x$ T_{exp}, where v is the velocity of the droplet and T_{exp} is the exposure time of the camera. As such, for a given velocity v, the optimal exposure time is determined to image the droplet at least twice as it moves *(2)*. Based on this mechanism described above. The acquired videos were processed with a custom workflow developed in MATLAB 2021a (Mathworks, Inc.) and computationally accelerated with a graphical processing unit (Nvidia GeForce ABC) to *a*) identify droplets containing microbeads, and *b*) determine if the substrate encapsulated within the droplet was enzymatically activated (**Figure 3**). First, each frame of the collected RGB videos was separated into red and blue color components, corrected for optical aberrations, and segmented by fluidic channel. Each segmented channel was then converted into a 1D intensity profile, $S_i^{B,R}$, where *i* is the index for the channel and B corresponds to the blue component of the image and R the red component of the image, by subtracting the frame background and integrating along the cross-section of the channel. Finally, the presence of beads and droplets within a channel was determined by analyzing the peaks in the cross correlation of $S_i^{B,R}$ with the corresponding MLS pattern scaled to match the streak length of the beads and droplets in each frame. Proper scaling of the MLS pattern for a channel, equivalent to identifying the velocity within that channel, was

accomplished by finding the maximum of the cross correlation between $S_i^{B,R}$ and the corresponding MLS patterns when scaled for streak lengths ranging from 1.6 mm to 9.6 mm. The subsequent peak detection algorithm was modified based on the Matlab findpeaks function. The thresholds for peak detection in the bead channel and the substrate channel were determined by flowing *a)* control samples without beads and *b)* control samples containing beads but not EVs respectively. A peak in the blue channel but not the red channel indicated a droplet with a bead without an EV, and a peak in both the blue and red channels indicated a positive droplet, *i.e.* a bead bound to a single EV. These quantities are stored for downstream AEVB calculations.

10-Channel droplet microfluidics device

A droplet microfluidic device with 10 parallel flow-focusing generators is fabricated using "double-sided imprinting" method, as previously reported(*5*). The microfluidic device contains four 200µm deep delivery channels, through which the fluids are distributed to individual droplet generators. The droplet generators are connected to the delivery channels by through-PDMS vias, with a depth of 150µm. The flow-focusing generators are designed to be 30 µm deep, matching the dimension of the flow-focusing nozzle. The channel dimensions are designed to satisfy the design criteria: $2N\left(\frac{R_d}{R_{dev}}\right) < 0.01$, where N is the number of the parallel devices, R_d and R_{dev} the fluidic resistance of the delivery channel and the device, respectively. The fluidic resistance of the channel can be calculated from $R = 12\left(\frac{\mu L}{wh^3}\right)\left(1 - 0.63\left(\frac{h}{w}\right)\right)^{-1}$, where µ is the viscosity of the fluid, and w,h,L are the width, height, and length of the channel, respectively. The design criteria ensure even fluid distribution throughout the devices since the fluidic resistance in the delivery channel is negligible, compared to that of the device channel.

Calculation of partitioning error

If we define *m* as the number of targets in sample, *n* as the total number of partitions, λ as the average number of targets per partition. Then we have

$$\lambda = \frac{m}{n}$$

If we define the percentage of empty partitions (E), based on binominal distribution (*6*) we could get $\quad \lambda = -\ln(E)$

Partitioning errors occur as targets may distribute differently among partitions from one experiment to the next. In a set of experiments, the number of empty partitions E would have variance that propagates to a corresponding variance in the calculated concentration λ (*6*). The partition error $u_p = \frac{\Delta m}{m} = \frac{\lambda_{max} - \lambda_{min}}{\lambda} = \frac{n(\lambda_{max} - \lambda_{min})}{n\lambda}$. Based on the model from Dube et al (*7*), λ_{min}

$= -\ln(E + Zc\sqrt{\frac{E(1-E)}{n}})$ while $\lambda_{max} = -\ln(E - Zc\sqrt{\frac{E(1-E)}{n}})$. If we consider $\sigma_E = \sqrt{\frac{E(1-E)}{n}}$). Then we get

$$u_p = \frac{\Delta m}{m} = \frac{\lambda_{max} - \lambda_{min}}{\lambda} = \frac{n(\lambda_{max} - \lambda_{min})}{n\lambda} = \frac{1}{\lambda}\ln(\frac{E + Zc\sigma_E}{E - Zc\sigma_E})$$

Assay Target	Platform	LOD (μL^{-1})	$AEVB_b$	Number of beads	Reference
iFN	SIMOA, Quanterix	210	1%	25,000	(*8*)
CD9-CD63 EVs	SIMOA, Quanterix	34	0.6%	25,000	(*9*)
iFN	Customized microarray	18	0.2-1%	60,000	(*8*)
CD63-GPC1 EVs	Customized microarray	10	Did not report	45,000	(*10*)
CD81-CD81	DEVA, µMD	9	0.023%	1,000,000	This work

Table S1

Comparing technical features of DEVA with commercial or research-based platforms to perform digital ELISA assays. Benefiting from its high throuput, DEVA can analyze a larger number of beads and achieves a low background level ($AEVB_b$).

Method	Number of compartments	Number of single EVs analyzed per assay	Reference
ddPCR	N/A	1,100	(11)
dELISA, SIMOA	25,000 microwells	2,500	(8, 12)
dELISA, customized microarray	20,000 microwells 1,000,000 droplets	4,500-10,000	(10, 13)
Droplet based dELISA	10,000,000 droplets	100,000	This work

Table S2
Comparing DEVA and typical commercial or research-based single EV analysis platforms that used digital assays. Based on DEVA's high throughput, more single EVs could be analyzed in one assay.
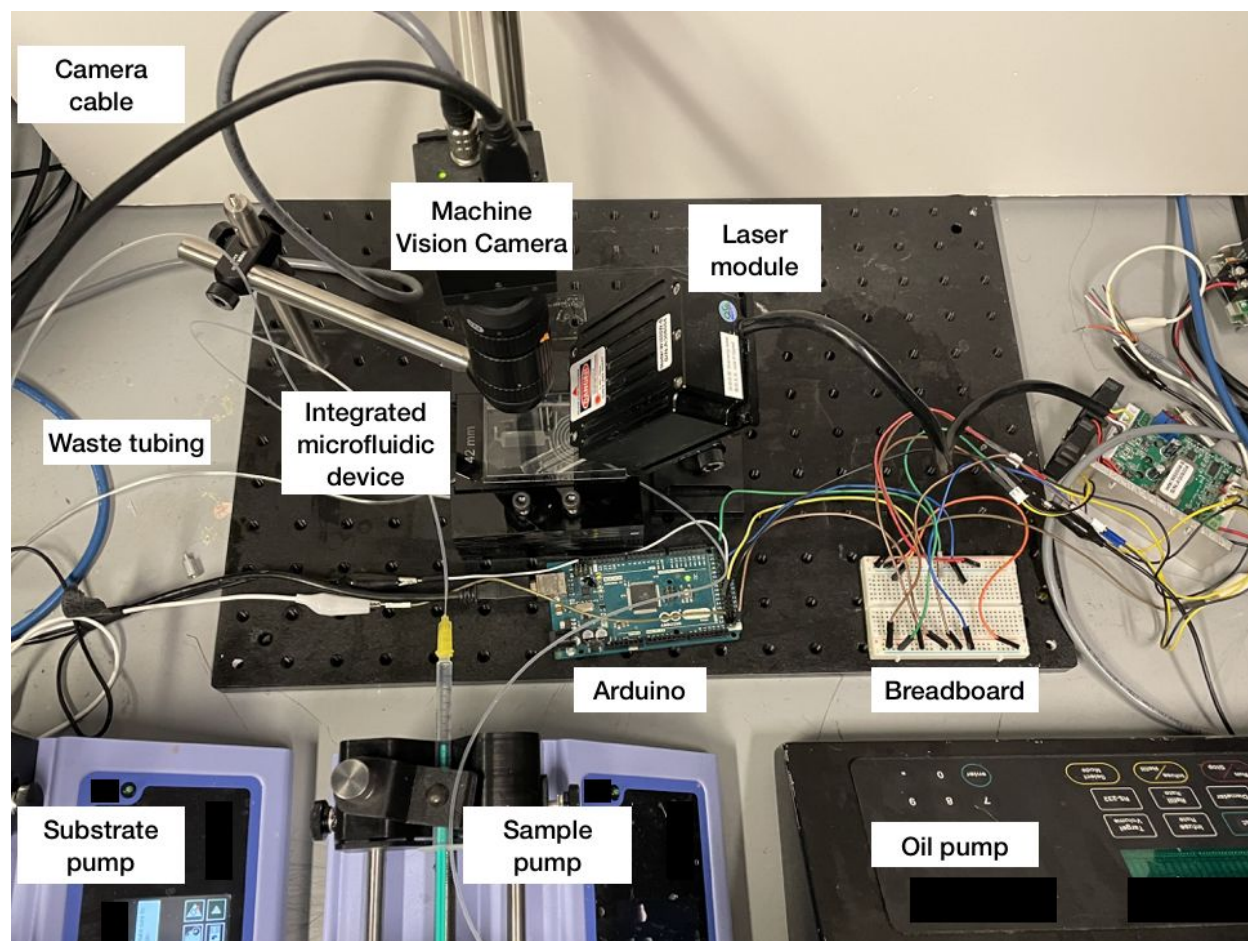
Figure S1. A photograph of the experimental setup of our DEVA platform
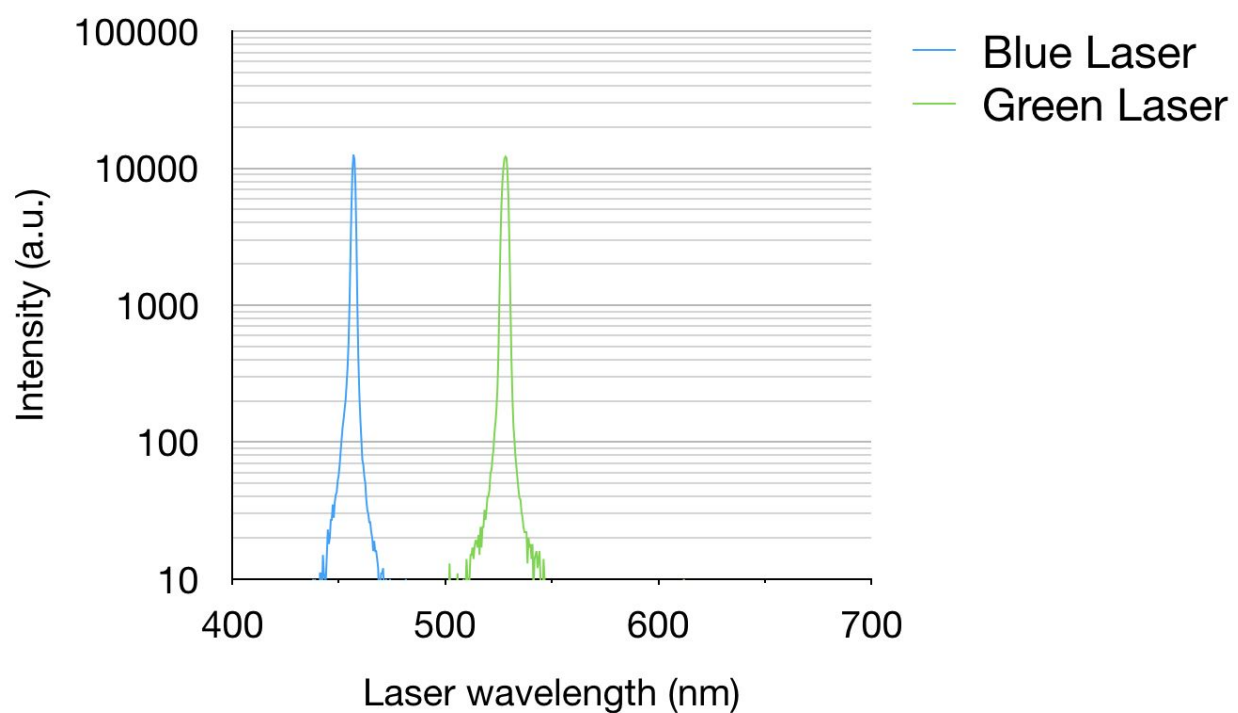
Figure S2. Excitation laser characterization for DEVA
A blue laser (λ_{exBlue} = 457 nm) was used to excite the signal from fluorescent microbeads while a green laser ($\lambda_{exGreen}$ = 528 nm) was used to excite the signal from fluorescent enzyme substrate.
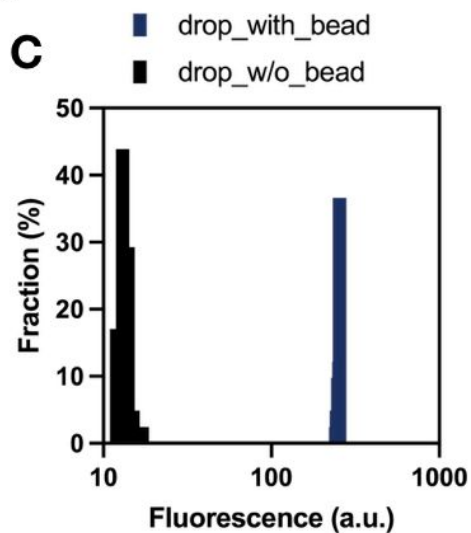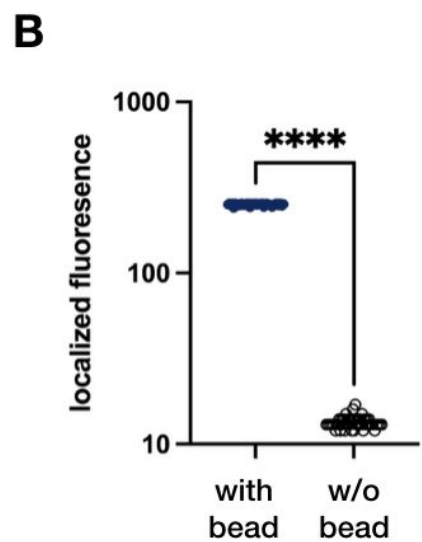
A

R² = 0.989

Detected bead number

10⁵
10⁴
10³
10²
0

10² 10³ 10⁴ 10⁵ 10⁶ 10⁷
Input bead number

B

localized fluoresence

1000

100

10

****

with bead | w/o bead

C

■ drop_with_bead
■ drop_w/o_bead

Fraction (%)

50
40
30
20
10

10 100 1000
Fluorescence (a.u.)

D

localized fluoresence

1000

100

10

****

with enzyme | w/o enzyme

E

■ drop_with_enzyme
■ drop_w/o_enzyme

Fraction (%)

100
10
1
0.1

10 100 1000
Fluorescence (a.u.)
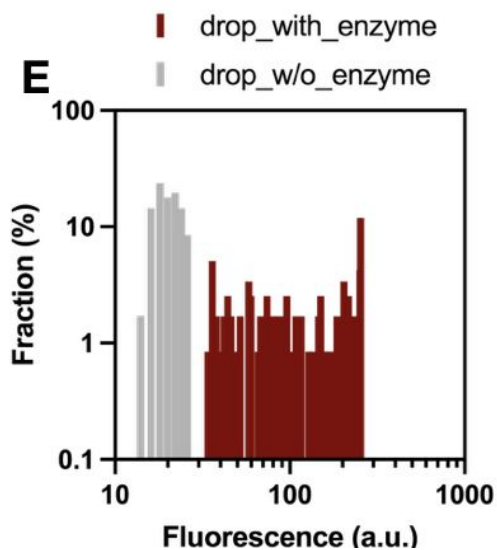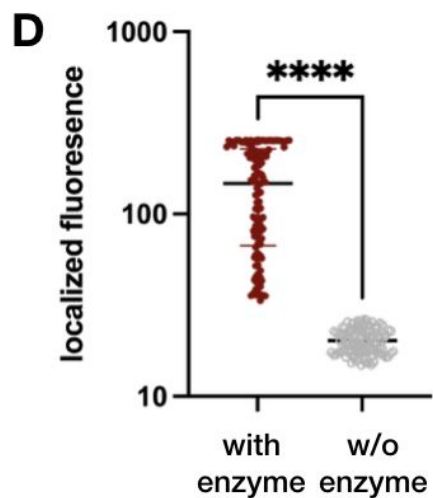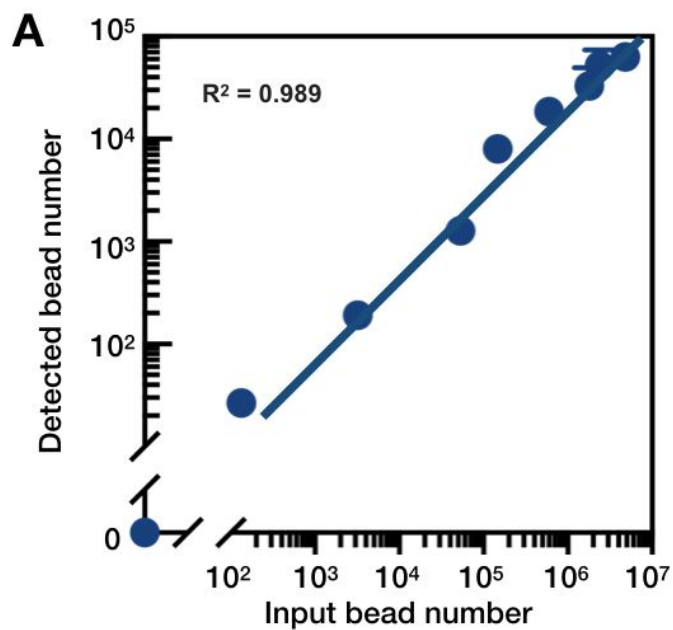
Figure S3. DEVA fluorescence characterization.
A. DEVA quantification of spiked-in beads, showing excellent linearity ($R^2 = 0.989$) over a large dynamic range (10^2-10^7). **B**. Comparison of the fluorescence intensity between droplets with beads versus those without (N=41). Welch's t-test was used to calculate the significance. **C**. Histogram showi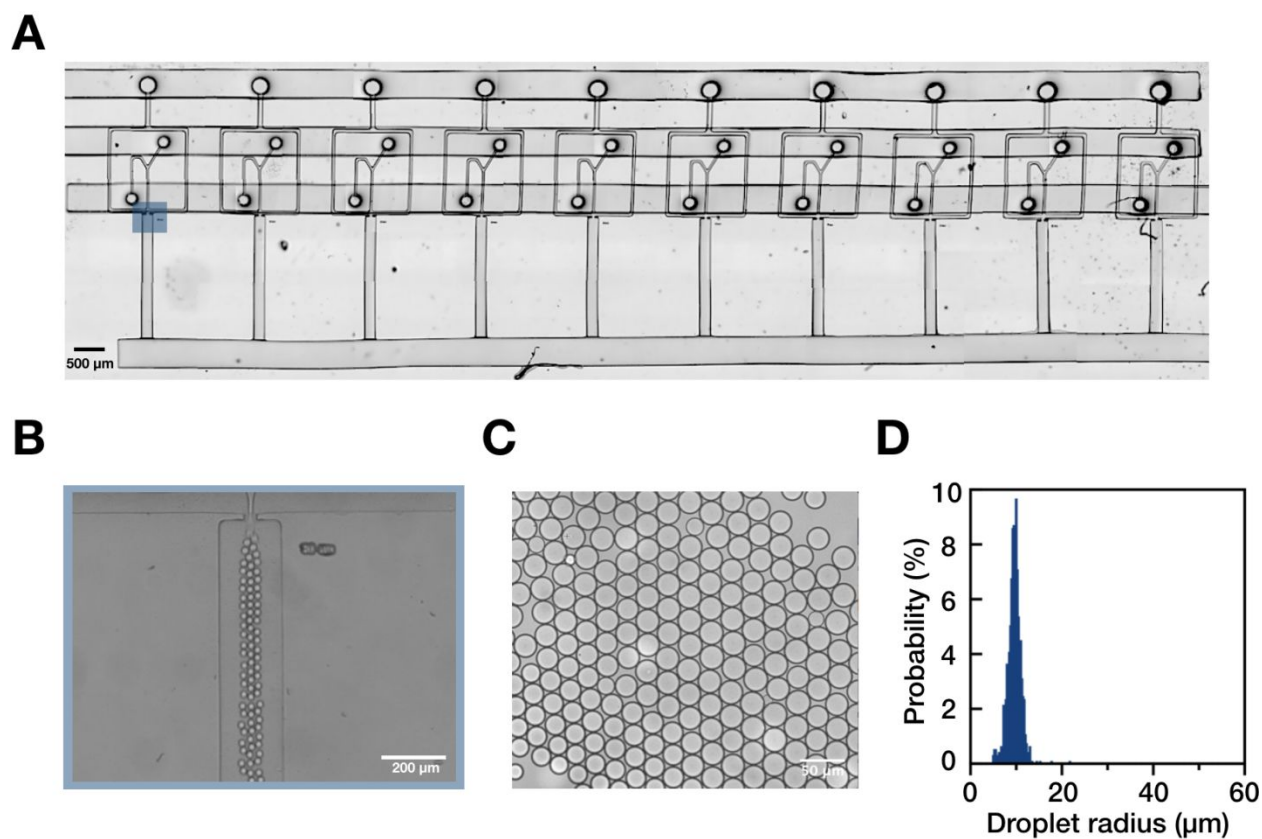ng the fluorescence intensity of droplets with and without fluorescent beads (N=41). **D**. Comparison of the fluorescence intensity between droplets with enzyme versus those without (N=118). Welch's t-test was used to calculate the significance. **E**. Histogram showing fluorescence intensity of droplets with and without enzyme (N=118).

Figure S4. **High throughput droplet generation enabled by parallelized flow focusing generators.**
 (A) Micrograph of a parallelized droplet generators in a ladder architecture fabricated in PDMS. Scale bar: 500µm. Navy box indicates the single droplet generator shown in B. (B) A micrograph of a single droplet generator making water in oil emulsions. Scale bar: 200µm. (C) A micrograph of the droplets generated by the ten parallelized droplet generators. Scale bar: 50µm. (D) A histogram of the diameter of the droplets collected from the parallelized droplet generation device. The flow rate for the combined aqueous phase is 4.6mL/hr and for the continuous flow rate of 60mL/hr.
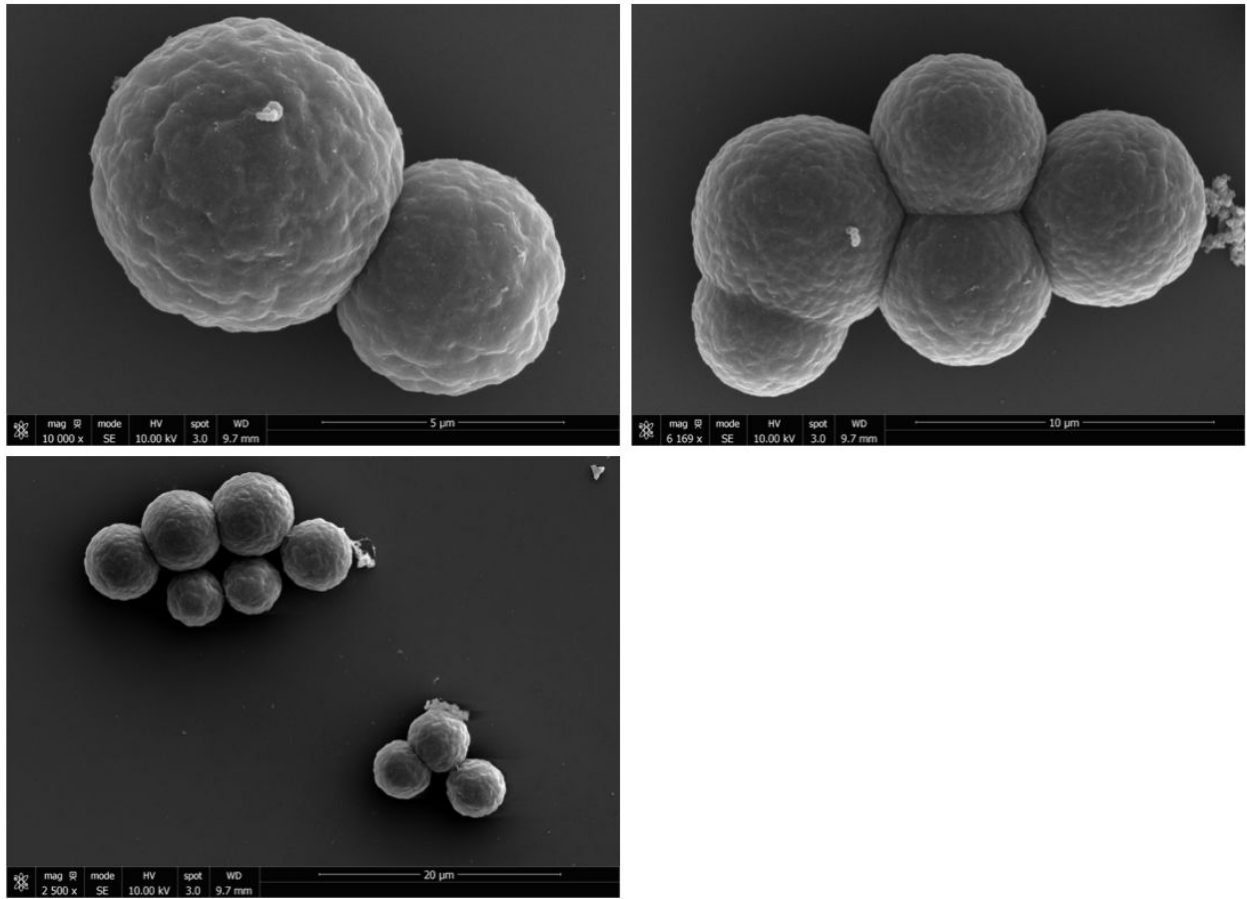
Figure S5. **SEM images of DEVA.**
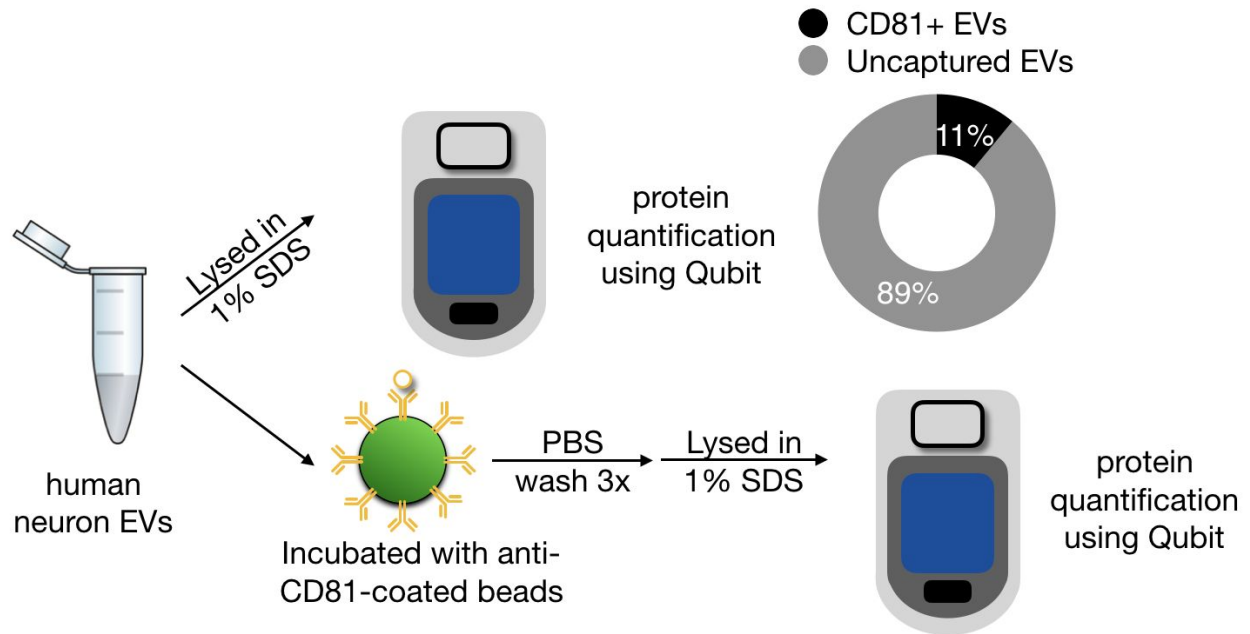SEM images showing immuno-captured single EV on bead.

Figure S6. **Schematics on determining the ratio of CD81+ EVs among the total human neuron EVs using Qubit protein assays.**
Isolated human neuron derived EVs were first lysed using 1% SDS buffer to measure the total EV protein cargo. Meanwhile, anti-CD81-coated beads were incubated with the same isolated human EVs to capture CD81^{+} EVs. After isolation and washing, CD81^{+} EVs that were captured on beads were lysed and measured using the same condition. After comparison, captured CD81^{+} EVs consist 11% of the protein cargo of human neuron derived EVs.
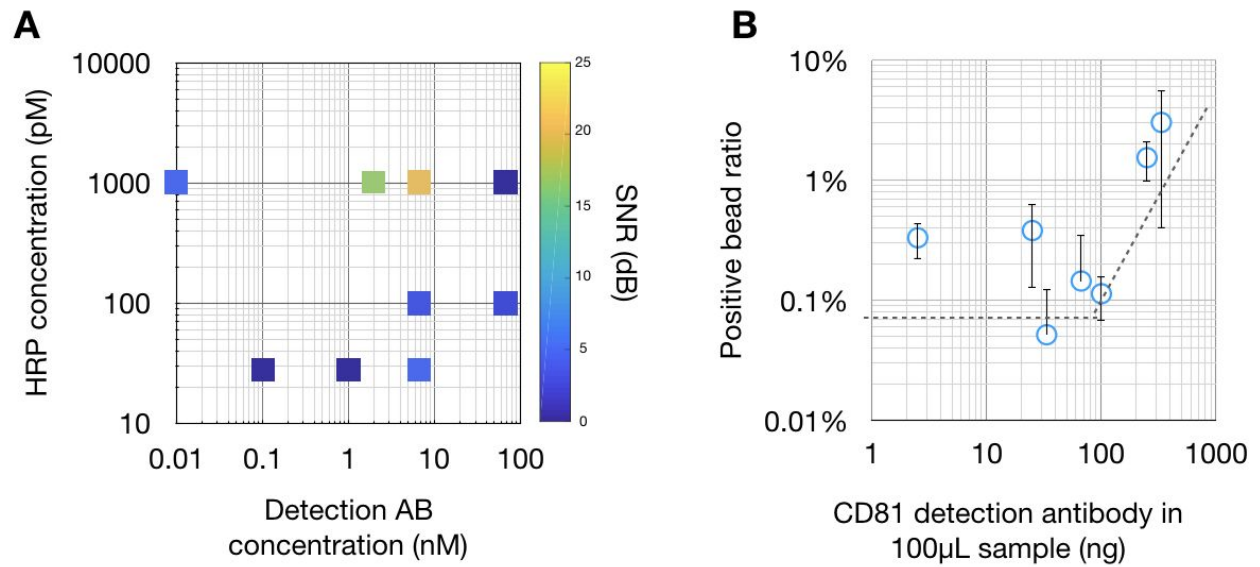
Figure S7. DEVA optimization on reagent concentration.
A. Several concentrations of HRP enzyme and detection antibody were evaluated for DEVA assay optimization. Each assay condition was applied to an EV-inputted and a blank sample, and a resulting SNR was calculated based on the number of positive droplets detected in the EV-inputted versus the blank sample. **B**. At 1nM HRP concentration, several detection antibody concentrations were added into blank samples without EVs to minimize unspecific binding. Error bars indicate standard deviation from replicates.
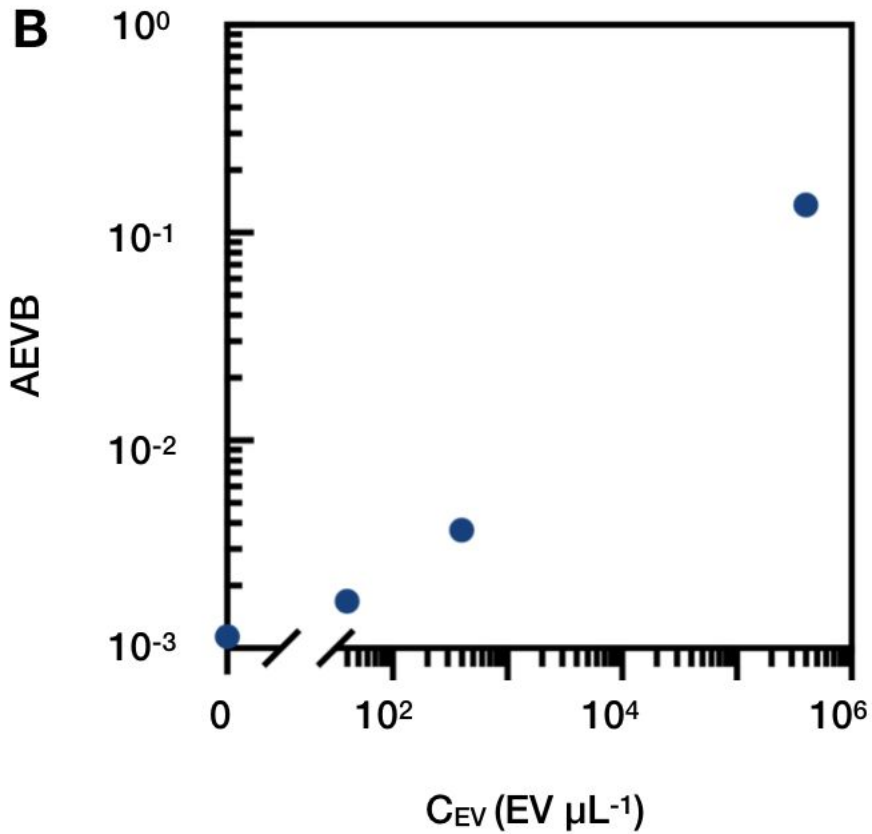
A

No EVs control   4x10^1 EV/µL   4x10^2 EV/µL   4x10^4 EV/µL
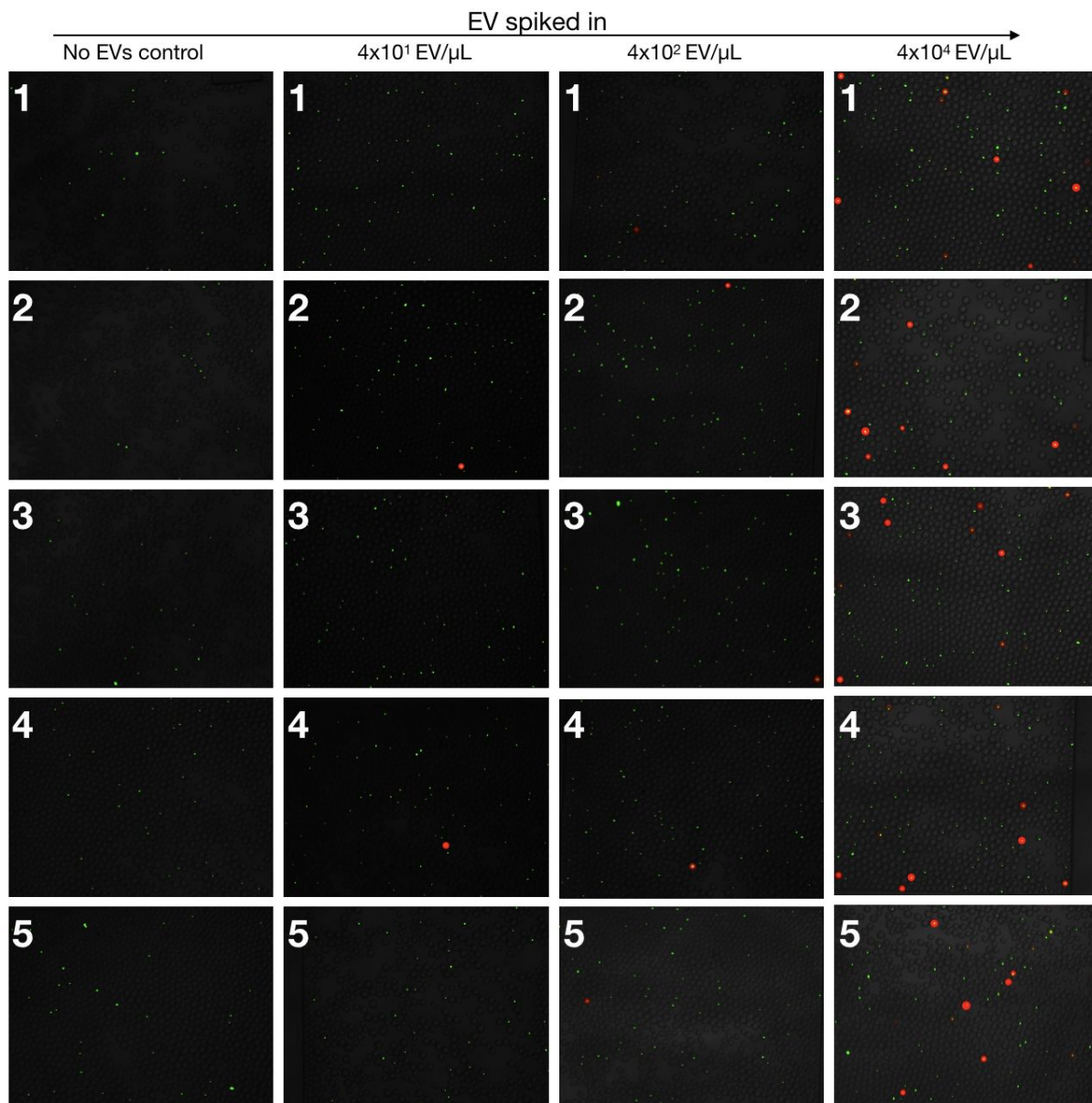
Figure S8. Supplementary fluorescent microscopic images.
A. Additional fluorescent microscopic images showing the DEVA assay on serially diluted human neuron EVs. Each experiment had over 30 images analyzed for AEVB calculation. **B.** Quantitative analysis of AEVB from fluorescent microscope images.
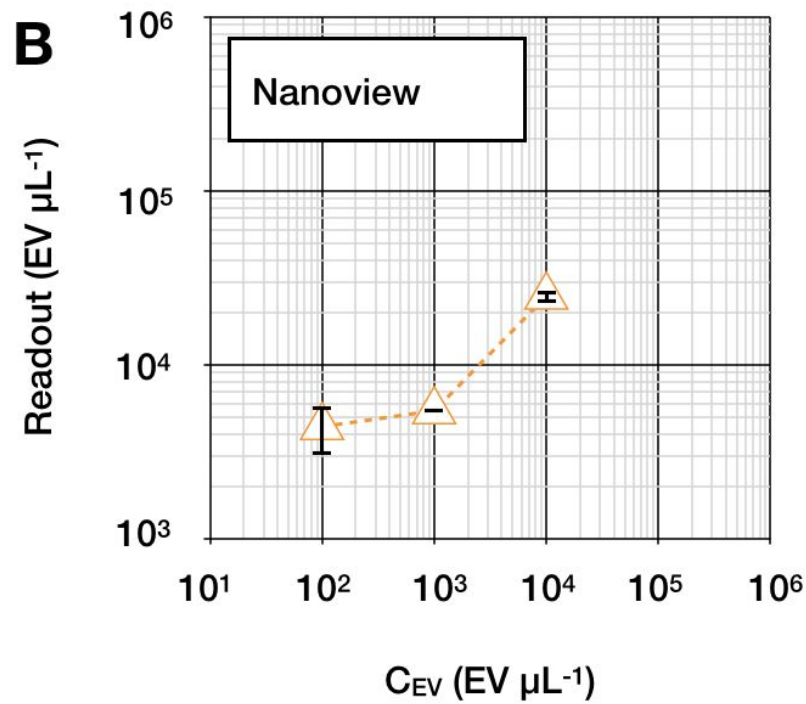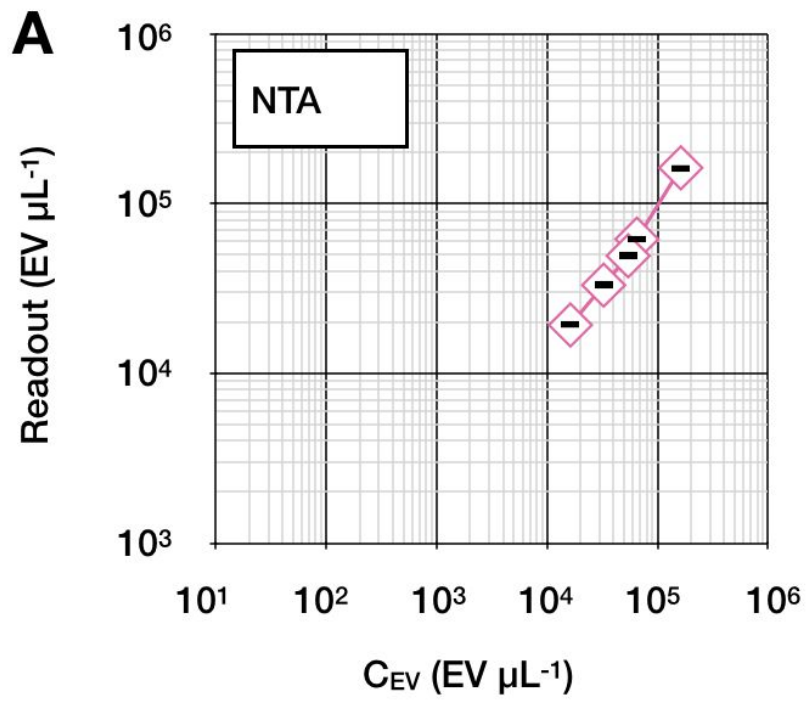
Figure S9. Human neuron EVs characterization on conventional tools. A. Isolated human neuron EVs characterized on Nanoparticle tracking analysis (NTA). **B**. Isolated human neuron EVs characterized on Nanoview platform. Error bars indicate standard deviation on both figures.
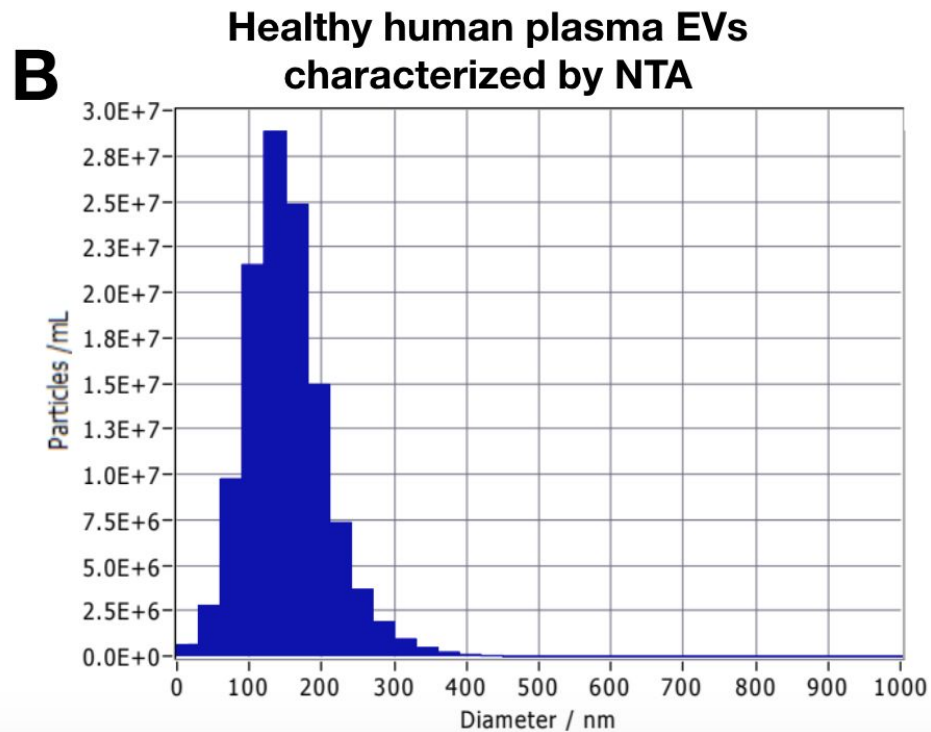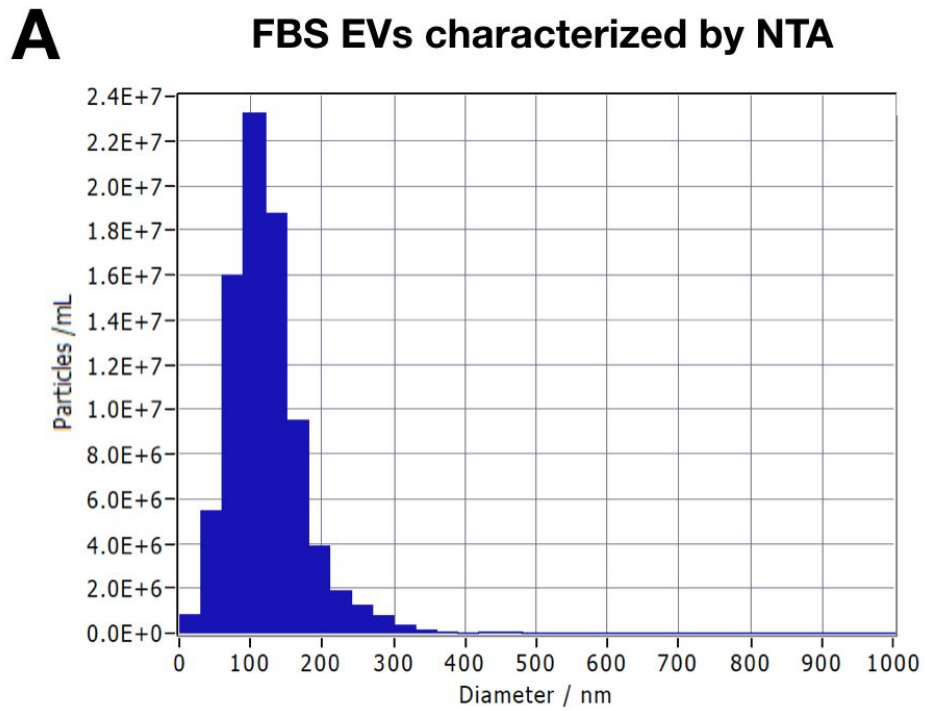
Figure S10. NTA analysis on isolated EVs.
A. NTA characterization on FBS EVs. **B**. NTA characterization on healthy human plasma EVs. EV number was calculated based on NTA result then spiked-in DEVA experiments.

Measuring human plasma EV using DEVA

We tested the feasibility of detecting endogenous EVs in a human plasma sample using DEVA (**Fig.S11**). Due to the presence of endogenous CD81+/CD81+ EVs in human plasma, we cannot do spike in experiments of known concentrations of target EVs into a background that contains no target EVs. Instead, we have validated the feasibility of detecting EVs in plasma by quantifying the number of $CD81^+/CD81^+$ EVs in human plasma at various dilutions. To validate the specificity of DEVA in human plasma, we compared these results to a negative control in which we replace the CD81 capture and label antibodies with an isotype antibody control (human IgG1, Miltenyi Biotec). In our measurements on DEVA, the isotype control showed consistent background at AEVB=0.134% (CV=15%) over three orders or magnitude of human plasma EV spiked-in the experiment.
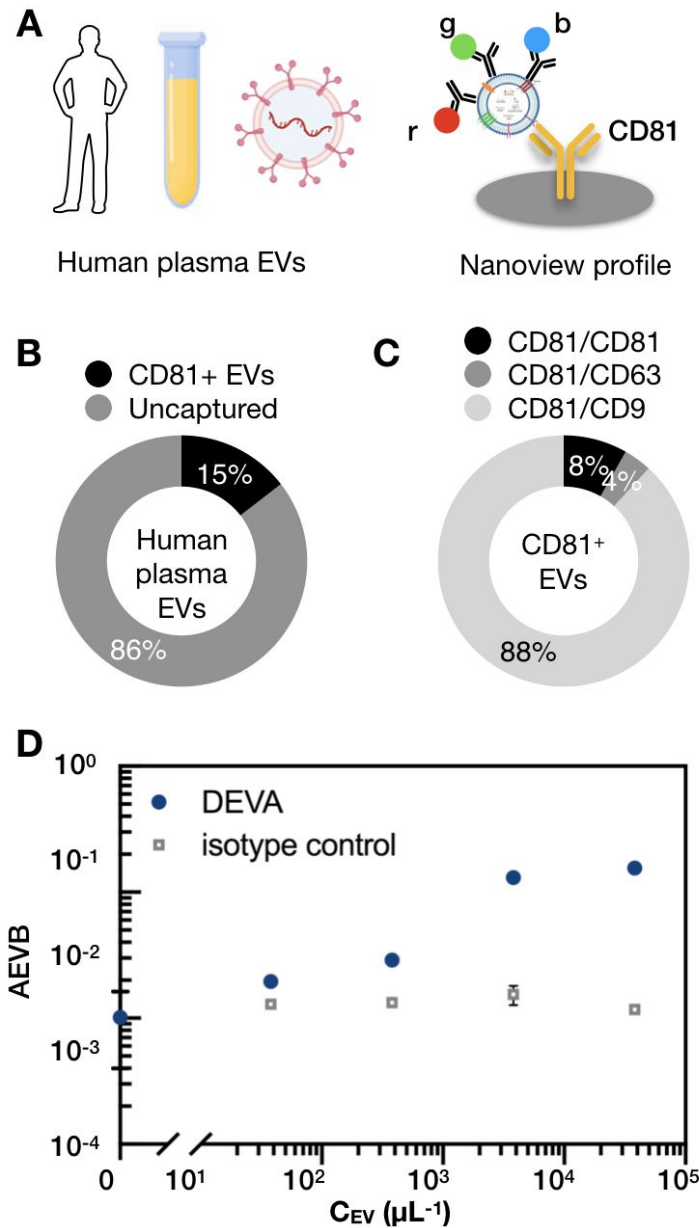
Figure S11. Feasibility of measuring endogenous EVs in human plasma using DEVA
A. Schematic of the measurements carried out on Nanoview to quantify the surface proteins expressed on human plasma EV by immunocapture and immunolabeling. **r** stands for CD63, **g** stands for CD81, **b** stands for CD9. Nanoview chip was coated by anti-CD81 antibody. **B**. We found that 15% of human plasma EVs express at least one CD81 protein based on immunoisolation and protein calibration. **C**. Surface protein profiling of CD81$^+$ EVs in human plasma by Nanoview. Among the CD81$^+$ EVs, 8% of them expressed at least one other CD81 protein. **D**. A titration curve for DEVA when endogenous human CD81/CD81 EVs are measured at various dilutions of 20µL of human plasma into 100µL sample volume. The x axis was estimated using NTA to measure human plasma $(1.2 \times 10^{12}/\text{mL})$, of which we assumed 1% were EVs based on prior literature(14). Our estimate of 1.2×10^{10} EVs/mL agrees with what has been previously reported in literature(14, 15). Error bars indicate standard deviations from replicates. Some error bars are too small to be seen on the figure.

REFERENCES

1. V. Yelleswarapu, J. R. Buser, M. Haber, J. Baron, E. Inapuri, D. Issadore, Mobile platform for rapid sub–picogram-per-milliliter, multiplexed, digital droplet detection of proteins. *Proc. Natl. Acad. Sci. U. S. A.* **116** (2019), doi:10.1073/pnas.1814110116.

2. V. R. Yelleswarapu, H.-H. Jeong, S. Yadavali, D. Issadore, Ultra-high throughput detection (1 million droplets per second) of fluorescent droplets using a cell phone camera and time domain encoded optofluidics. *Lab Chip*. **17**, 1083–1094 (2017).

3. Y. Zhang, C. H. Pak, Y. Han, H. Ahlenius, Z. Zhang, S. Chanda, S. Marro, C. Patzke, C. Acuna, J. Covy, W. Xu, N. Yang, T. Danko, L. Chen, M. Wernig, T. C. Südhof, Rapid single-step induction of functional neurons from human pluripotent stem cells. *Neuron*. **78** (2013), doi:10.1016/j.neuron.2013.05.029.

4. J. P. Dollé, A. Jaye, S. A. Anderson, H. Ahmadzadeh, V. B. Shenoy, D. H. Smith, Newfound sex differences in axonal structure underlie differential outcomes from in vitro traumatic axonal injury. *Exp. Neurol.* **300** (2018), doi:10.1016/j.expneurol.2017.11.001.

5. H. H. Jeong, S. Yadavali, D. Issadore, D. Lee, Liter-scale production of uniform gas bubbles: Via parallelization of flow-focusing generators. *Lab Chip*. **17** (2017), doi:10.1039/c7lc00295e.

6. F. Bizouarn, Introduction to digital PCR. *Methods Mol. Biol.* **1160** (2014), doi:10.1007/978-1-4939-0733-5_4.

7. S. Dube, J. Qin, R. Ramakrishnan, Mathematical analysis of copy number variation in a DNA sample using digital PCR on a nanofluidic device. *PLoS One*. **3** (2008), doi:10.1371/journal.pone.0002876.

8. L. Cohen, N. Cui, Y. Cai, P. M. Garden, X. Li, D. A. Weitz, D. R. Walt, Single Molecule Protein Detection with Attomolar Sensitivity Using Droplet Digital Enzyme-Linked Immunosorbent Assay. *ACS Nano*. **14** (2020), doi:10.1021/acsnano.0c02378.

9. P. Wei, F. Wu, B. Kang, X. Sun, F. Heskia, A. Pachot, J. Liang, D. Li, Plasma

extracellular vesicles detected by Single Molecule array technology as a liquid biopsy for colorectal cancer. *J. Extracell. Vesicles*. **9** (2020), doi:10.1080/20013078.2020.1809765.

10.   C. Liu, X. Xu, B. Li, B. Situ, W. Pan, Y. Hu, T. An, S. Yao, L. Zheng, Single-Exosome-Counting Immunoassays for Cancer Diagnostics. *Nano Lett.* **18**, 4226–4232 (2018).

11.   J. Ko, Y. Wang, K. Sheng, D. A. Weitz, R. Weissleder, Sequencing-Based Protein Analysis of Single Extracellular Vesicles. *ACS Nano*. **15** (2021), doi:10.1021/acsnano.1c00782.

12.   F. Wu, Y. Gu, B. Kang, F. Heskia, A. Pachot, M. Bonneville, P. Wei, J. Liang, PD-L1 detection on circulating tumor-derived extracellular vesicles (T-EVs) from patients with lung cancer. *Transl. Lung Cancer Res.* **10** (2021), doi:10.21037/tlcr-20-1277.

13.   Q. Tian, C. He, G. Liu, Y. Zhao, L. Hui, Y. Mu, R. Tang, Y. Luo, S. Zheng, B. Wang, Nanoparticle Counting by Microscopic Digital Detection: Selective Quantitative Analysis of Exosomes via Surface-Anchored Nucleic Acid Amplification. *Anal. Chem.* **90** (2018), doi:10.1021/acs.analchem.8b00189.

14.   K. B. Johnsen, J. M. Gudbergsson, T. L. Andresen, J. B. Simonsen, What is the blood concentration of extracellular vesicles? Implications for the use of extracellular vesicles as blood-borne biomarkers of cancer. *Biochim. Biophys. Acta - Rev. Cancer*. **1871** (2019), , doi:10.1016/j.bbcan.2018.11.006.

15.   S. Jamaly, C. Ramberg, R. Olsen, N. Latysheva, P. Webster, T. Sovershaev, S. K. Brækkan, J. B. Hansen, Impact of preanalytical conditions on plasma concentration and size distribution of extracellular vesicles using Nanoparticle Tracking Analysis. *Sci. Rep.* **8** (2018), doi:10.1038/s41598-018-35401-8.